ЖЭТФ, 2012, том 141, вып. 2, стр. 387–398

THE FERMI–PASTA–ULAM RECURRENCE AND RELATED PHENOMENA FOR $1D$ SHALLOW-WATER WAVES IN A FINITE BASIN

V. P. Ruban*

Landau Institute for Theoretical Physics, Russian Academy of Sciences
119334, Moscow, Russia

Received April 5, 2011

Different regimes of the Fermi–Pasta–Ulam (FPU) recurrence are simulated numerically for fully nonlinear "one-dimensional" potential water waves in a finite-depth flume between two vertical walls. In such systems, the FPU recurrence is closely related to the dynamics of coherent structures approximately corresponding to solitons of the integrable Boussinesq system. A simplest periodic solution of the Boussinesq model, describing a single soliton between the walls, is presented in analytic form in terms of the elliptic Jacobi functions. In the numerical experiments, it is observed that depending on the number of solitons in the flume and their parameters, the FPU recurrence can occur in a simple or complicated manner, or be practically absent. For comparison, the nonlinear dynamics of potential water waves over nonuniform beds is simulated, with initial states taken in the form of several pairs of colliding solitons. With a mild-slope bed profile, a typical phenomenon in the course of evolution is the appearance of relatively high (rogue) waves, while for random, relatively short-correlated bed profiles it is either the appearance of tall waves or the formation of sharp crests at moderate-height waves.

1. INTRODUCTION

Nearly integrable wave systems are known to exhibit the Fermi–Pasta–Ulam (FPU) recurrence, when a (finite-size) system approximately repeats its initial state after some period of evolution. Starting from the first observation of this phenomenon in the famous numerical experiment with one-dimensional ($1D$) lattices of nonlinear oscillators [1], the FPU recurrence and related phenomena were studied in many physical contexts (see, e.g., Refs. [2–14] and the references therein). In particular, Zabusky and Kruskal [2] discovered solitons with a highly nontrivial behavior, when numerically investigated a mechanism of the recurrence for spatially periodic solutions of the Korteweg–de Vries (KdV) equation. Presently, the theory of solitons has developed into one of the main branches of nonlinear science.

It is well known that many integrable mathematical models have their origin in the theory of water waves. The two most famous integrable equations are the KdV equation, first derived for weakly dispersive unidirectional shallow-water waves, and the nonlinear Schrödinger equation, which describes an envelope of a train of deep-water waves [15]. For deep-water waves, many analytic and experimental results concerning the FPU recurrence are known [4–9, 16–19]. As regards the shallow-water regime, only some numerical studies for the KdV equation and its higher-order generalizations were performed until recently (see, e.g., Refs. [10, 11]), while the FPU phenomenon was never considered theoretically for long waves in a finite flume, and was never studied experimentally in the shallow-water regime.

It is clear that the KdV equation is not adequate for long waves in a finite basin where they reflect from the walls. Fortunately, there is another integrable model, the Boussinesq system, that approximately describes bidirectional shallow-water waves and is therefore potentially useful for analytic study of the FPU recurrence in a finite-length flume (concerning the integrability of the Boussinesq system, see Refs. [20–23], and concerning the deviations of water waves from exact integrability, see Refs. [10, 24]). Presently, however, we do not have a clear theory of FPU recurrence for shallow water, based on the Boussinesq system. Perhaps, a future theory should be built with the help of the sophisticated mathematical methods developed for

*E-mail: ruban@itp.ac.ru

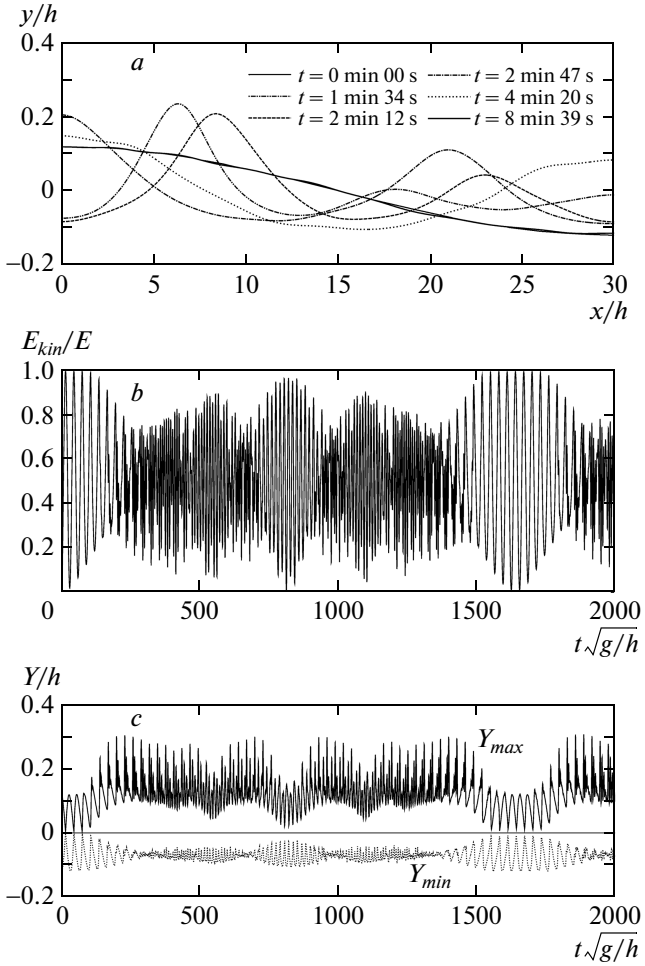

Fig. 1. The FPU recurrence is perfect with the initial shape of the free surface in the form $\eta_0(x) = 0.12h\cos(2\pi x/60h)$ with $L/h = 60$, $A_0/h = 0.12$, and $h = 1.0$ m: a — wave profiles at several time moments when the kinetic energy is at a minimum; b — the ratio of the kinetic energy to the total energy; c — the maximum and minimum elevations of the free boundary

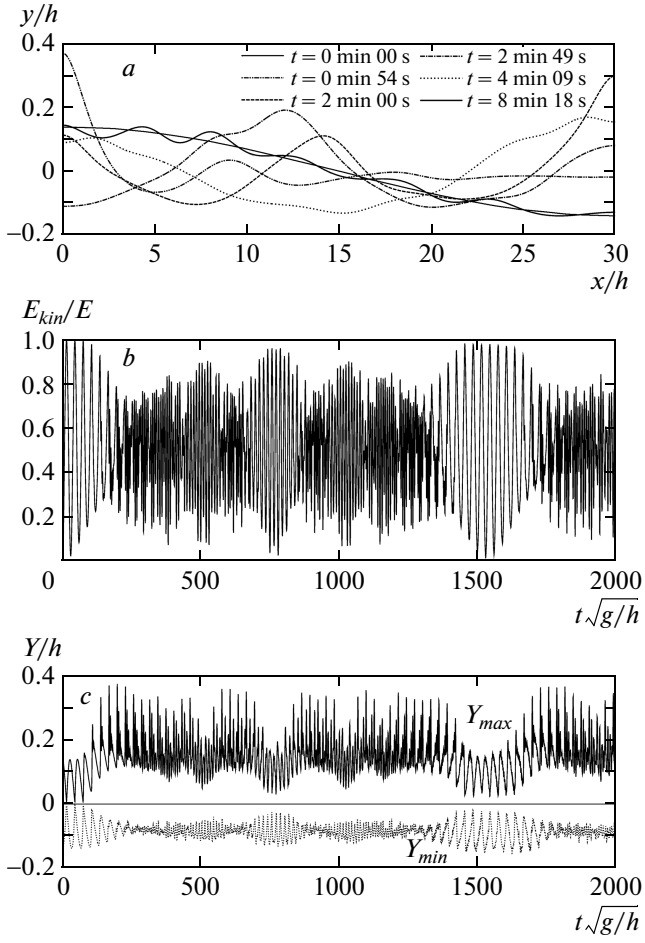

Fig. 2. The FPU recurrence is less perfect with a larger initial amplitude, $\eta_0(x) = 0.14h\cos(2\pi x/60h)$ with $L/h = 60$, $A_0/h = 0.14$, and $h = 1.0$ m, because the nonintegrability effects are stronger (a, b, and c show the same quantities as in Fig. 1)

obtaining spatially periodic solutions of integrable systems (in particular, see [22] for the Boussinesq model). In this paper, such a general purpose is not achieved, although a family of periodic solutions is derived in an explicit analytic form using a simple ansatz that corresponds to a single soliton periodically moving between the walls. However, that solution is by no means the main result of our work; it just plays an auxiliary role, namely, to provide nearly "many-soliton" initial conditions for highly accurate numerical experiments.

Very recently, our short paper was published where for the first time the FPU recurrence was studied numerically for fully nonlinear shallow-water waves in a finite flume [25]. Exact equations of motion for potential planar flows of a perfect fluid with a free surface in terms of so-called conformal variables were used in that study [26, 27]. The simplest initial states were taken, with zero velocity field and a cosine-shaped free boundary. Two typical examples of the recurrence are presented in Figs. 1 and 2.

One of the purposes of this paper is to provide additional numerical examples of the recurrence for different initial states, and to demonstrate a relation of the FPU phenomenon in shallow-water finite basins to solitons of the approximate Boussinesq system. Another purpose is to observe what new effects appear in the dynamics of long dispersive waves if the bottom boundary is nonuniform (it should be noted that conformal vari-

ables provide exact equations of motion for an arbitrary nonuniform bottom profile when it is parameterized by an analytic function [26, 27]). In particular, three kinds of bed profiles are considered: mild-slope beds, beds with quasirandom, relatively short-correlated corrugations, and beds with randomly placed barriers. The nonuniformity destroys the approximate integrability, and therefore initial states in the form of several pairs of colliding solitons evolve to the appearance of highly nonlinear wave events. Such steep and tall waves can be considered a $1D$ model for freak (rogue) waves sometimes arising in the coastal zone (the subject of freak waves is currently studied very extensively, see [28–30] and the references therein).

2. DIFFERENT EXAMPLES OF THE FPU RECURRENCE

2.1. Notes about the numerical method

We consider two-dimensional ($2D$) potential flows of a perfect fluid with the velocity field

$$\mathbf{v}(x,y,t) = \nabla\varphi(x,y,t),$$

where x is the horizontal coordinate, y is the vertical coordinate, and t is the time. The velocity potential φ satisfies the $2D$ Laplace equation $\varphi_{xx} + \varphi_{yy} = 0$ inside the flow domain, with the condition of zero normal velocity $\partial\varphi/\partial n = 0$ at a (fixed) bottom boundary. At the free surface $y = \eta(x,t)$, where the normal velocity is $V_n = (\partial\varphi/\partial n)_{y=\eta}$, we have two basic equations of motion, the so-called kinematic boundary condition and the dynamic boundary condition (the Bernoulli equation):

$$\eta_t - V_n\sqrt{1+\eta_x^2} = 0, \tag{1}$$

$$(\varphi_t + \mathbf{v}^2/2 + gy)_{y=\eta} = 0, \tag{2}$$

where g is the gravity acceleration (we neglect the surface tension in this work).

Because the boundaries are nonuniform, Cartesian coordinates are not convenient for an exact treatment of the above problem. Fortunately, the $2D$ Laplace equation is invariant under conformal transformations of independent variables, and it is therefore possible to introduce time-dependent conformal coordinates $\vartheta(x,y,t)$ and $\nu(x,y,t)$ such that the flow domain corresponds to a horizontal stripe $0 \le \nu \le \alpha(t)$ in the $\vartheta\nu$ plane (for details, see Refs. [26, 27]). In the conformal variables, the potential $\varphi(\vartheta,\nu,t)$ satisfies the Laplace equation $\varphi_{\vartheta\vartheta} + \varphi_{\nu\nu} = 0$, with simple boundary conditions $\varphi_\nu(\vartheta,0,t) = 0$ and $\varphi(\vartheta,\alpha(t),t) = \psi(\vartheta,t)$.

The conformal variables result in a parameterization of the (x-periodic) free surface in terms of a real function $\rho(\vartheta,t)$ as follows [26, 27]:

$$X + iY = Z\left[\vartheta + i\alpha(t) + \left(1 + i\hat{R}_\alpha\right)\rho(\vartheta,t)\right], \tag{3}$$

where $\hat{R}_\alpha$ is a linear integral operator diagonal in the discrete Fourier representation, $R_\alpha(m) = i\,\mathrm{th}(\alpha m)$ (here, m is the number of a Fourier harmonic). A fixed analytic function $Z(\zeta)$ determines a conformal mapping of a sufficiently wide horizontal stripe in the upper half-plane of an auxiliary complex variable ζ, adjacent to the real axis $\mathrm{Im}\,\zeta = 0$, onto a region in the physical xy plane, with the real axis $\mathrm{Im}\,\zeta = 0$ parameterizing the bed profile.

Exact compact expressions for the time derivatives $\rho_t(\vartheta,t)$, $\psi_t(\vartheta,t)$, and $\dot{\alpha}(t)$ were obtained, corresponding to the dynamics of potential water waves in the uniform gravity field [26, 27]:

$$\rho_t = -\,\mathrm{Re}[\xi_\vartheta(\hat{T}_\alpha + i)Q], \tag{4}$$

$$\psi_t = -\,\mathrm{Re}[\Phi_\vartheta(\hat{T}_\alpha + i)Q] - \frac{|\Phi_\vartheta|^2}{2|Z'(\xi)\xi_\vartheta|^2} - g\,\mathrm{Im}\,Z(\xi), \tag{5}$$

$$\dot{\alpha}(t) = -\frac{1}{2\pi}\int_0^{2\pi} Q(\vartheta)\,d\vartheta, \tag{6}$$

where

$$\xi = \vartheta + i\alpha + (1 + i\hat{R}_\alpha)\rho, \quad \Phi = (1 + i\hat{R}_\alpha)\psi,$$

$$Q = \frac{\hat{R}_\alpha\psi_\vartheta}{|Z'(\xi)\xi_\vartheta|^2}.$$

The operator $\hat{T}_\alpha$ is diagonal in the discrete Fourier representation:

$$T_\alpha(m) = -i\,\mathrm{cth}(\alpha m), \quad m \ne 0,$$

$$T_\alpha(0) = 0.$$

Equation (4) is the kinematic boundary condition at the free surface, written in terms of conformal variables, Eq. (5) is the dynamic boundary condition (the Bernoulli equation), and Eq. (6) takes the time dependence of the conformal depth α into account, which is necessary for the conservation of the total fluid volume.

If the function $Z(\zeta)$ is expressed in terms of elementary analytic functions (such as $\exp(\dots)$, $\log(\dots)$,

and so on; see [26, 27, 31–33] for particular examples), then the right-hand sides of Eqs. (4)–(6) can be easily evaluated using the fast Fourier transform routines and mathematical library complex functions (in C programming language, the names of such complex functions are $\mathrm{c}\exp(\dots)$, $\mathrm{c}\log(\dots)$, and so on). The above properties form the base of the numerical method.

In the numerical experiments, we use dimensionless variables (however, for graphical presentations, the wave profiles are rescaled to a characteristic depth $h = 1$ m), and consider either flat horizontal or 2π-periodic nonuniform bed profiles (which means $Z(\zeta + 2\pi) = 2\pi + Z(\zeta)$) having an additional symmetry about the imaginary axis,

$$\operatorname{Im} Z(-\zeta' + i\zeta'') = \operatorname{Im} Z(\zeta' + i\zeta''),$$

$$\operatorname{Re} Z(-\zeta' + i\zeta'') = -\operatorname{Re} Z(\zeta' + i\zeta'').$$

This symmetry is required for simulations of waves between the vertical walls located at $x = 0$ and at $x = \pi$. Of course, the functions $\psi(\vartheta, t)$ and $\rho(\vartheta, t)$ should also have definite symmetries:

$$\psi(\vartheta + 2\pi, t) = \psi(\vartheta, t), \quad \psi(-\vartheta, t) = \psi(\vartheta, t),$$

$$\rho(\vartheta + 2\pi, t) = \rho(\vartheta, t), \quad \rho(-\vartheta, t) = -\rho(\vartheta, t).$$

The symmetries are automatically preserved in time if the initial data are symmetric.

In all our simulations, the system at $t = 0$ is characterized by a free surface profile $y = \eta_0(x)$ and by the velocity field $\mathbf{v} = 0$. Such initial conditions with zero kinetic energy E_{kin} were taken because they are convenient to observe the recurrence by monitoring the time dependence of the quantity E_{kin}/E, where E is the total energy, which is conserved in the numerical experiments up to 7–8 decimal digits. The function $\eta_0(x)$ is even and periodic, and therefore satisfies the boundary conditions $\eta_0'(0) = \eta_0'(L/2) = 0$, where L is an x-period. A special procedure was designed to numerically find the function $\rho(\vartheta, 0)$ corresponding to a given initial profile $\eta_0(x)$ [25].

2.2. Example where the recurrence is absent

We stress that the FPU recurrence occurs for special initial conditions only. It is clear from the theoretical standpoint that the recurrence corresponds to a nearly closed trajectory on a torus in the phase space of an integrable system. The dimensionality of the torus is equal to the number of the effectively excited degrees of freedom. Typically, the frequencies of that motion are not rationally related. Therefore, recurrence is not observed in the generic case. In Fig. 3, as an example of the case where the recurrence is practically absent, we present the evolution of some relevant parameters in the numerical experiment with

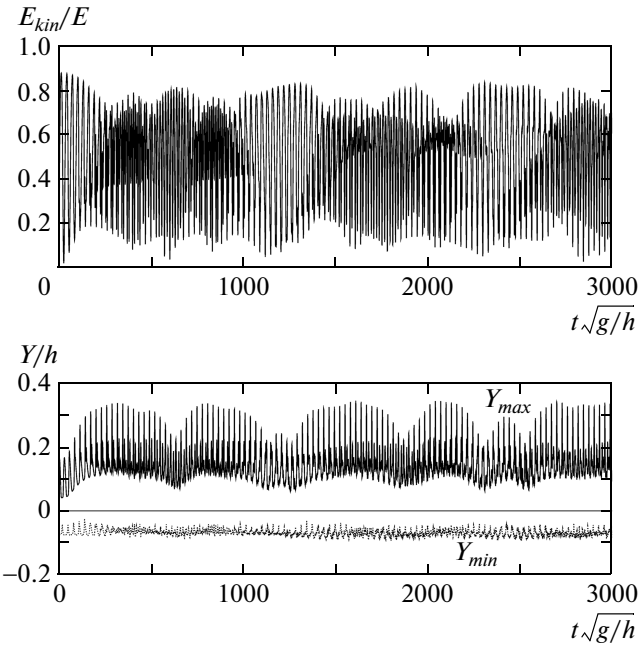

Fig. 3. The FPU recurrence is practically absent when $\eta_0(x) = 0.24h\{[1 + \cos(2\pi x/60h)]^3/8 - 5/16\}$

$$\eta_0(x) = 0.24h\left[\frac{1}{8}\left(1 + \cos\frac{2\pi x}{60h}\right)^3 - \frac{5}{16}\right].$$

From this standpoint, it may seem miraculous that the initial profiles in the simplest form $\eta_0(x) = A_0\cos(2\pi x/L)$ demonstrate rather perfect recurrences despite a fairly large number of the effectively excited degrees of freedom, $N_s = 5, 6, 7$ for $A_0/h = 0.12$ and $L/h = 100, \dots, 120$, as in the numerical experiments reported in [25].

2.3. Recurrence in the dynamics of solitons

It is well-known that integrable systems with periodic boundary conditions have so-called finite-gap solutions, which are exactly finite-dimensional subsystems with the dynamics on a torus. For the Boussinesq system, the simplest example is given in the Appendix and more involved cases are considered in Ref. [22]. In the general case, the formulas are quite complicated, and it is difficult to describe the corresponding degrees of freedom in terms of simple physical quantities. However, if the x-period is sufficiently long, an approxi-

mate description in terms of several colliding solitons becomes possible. In the Boussinesq model, "free" solitons are characterized by positive or negative dimensionless velocities s_n (constant and all different) and by the positions (phases) $x_n(t)$. The corresponding analytic solutions are presented in [23]. It is important that when two solitons with opposite velocities $s_1 = -s_2 = s$ collide at a position x_0 (or a single soliton collides with the wall), the velocity field along the flow domain is identically zero at some time moment, while the shape of the free surface is given by the simple formula $\eta(x) = \mathcal{S}(x - x_0, s)$ with

$$\mathcal{S}(x - x_0, s) = \frac{2h(s^2 - 1)}{\mathrm{ch}^2[\sqrt{3(s^2 - 1)}(x - x_0)/2h]}. \qquad (7)$$

This formula was used in our numerical experiments to prepare initial states in the form of several pairs of colliding solitons, placed sufficiently far apart from each other.

In a finite domain, each soliton moves between the walls and additionally acquires a definite phase shift $\sigma(s_n)$ when it reflects from a wall ($s_n \to -s_n$ after reflection) and phase shifts $\Delta(s_n, s_m)$ when it collides with other solitons [23]. In this picture, the recurrence occurs when the positions of all solitons self-consistently return close to their initial values at some time moment. The simplest nontrivial example of a quasirecurrence in the system of two solitons is shown in Fig. 4.

But the above approximate description does not work if we initially put several identical humps, each corresponding to a pair of colliding solitons, at different positions. Figure 5 shows that the recurrence occurs in a more complicated way in such a case.

If we put two or more humps, with one of them higher than the others, then the recurrence is possible only with tuned values of the larger velocity. Successful examples are shown in Figs. 6 and 7.

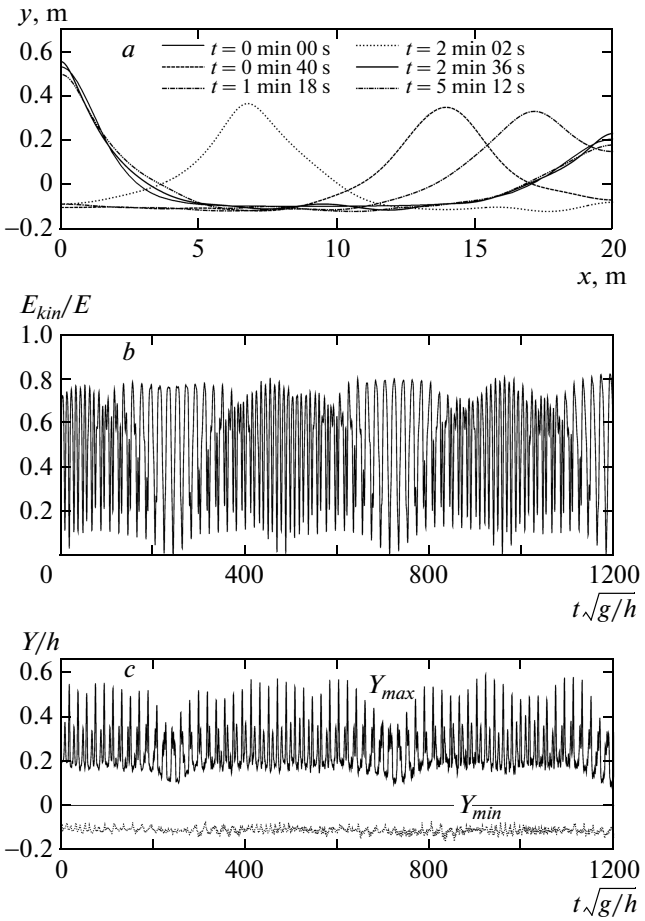

Fig. 4. Example of the FPU recurrence when two solitons with different parameters are present in the system ($L = 40$ m, $h = 1.0$ m; *a*, *b*, and *c* show the same quantities as in Fig. 1)

3. EXTREME WAVES OVER NONUNIFORM BEDS

We have observed in numerical experiments that with a flat bottom, if all the initial humps are nearly of the same height, the maximum surface elevation, as a function of time, does not much exceed the initial value for a long time. What happens if the bed is nonuniform? This question is answered in this section based on a set of numerical experiments. Three typical examples are presented below.

In the first nonuniform case, we simulated waves over a mild-slope bottom, corresponding to a function $Z(\zeta)$ of the form (Fig. 8)

$$Z_1(\zeta) = \zeta + \frac{2\pi i}{400}\left(0.2e^{i\zeta} - 1\right). \qquad (8)$$

The initial state was eight pairs of colliding solitons placed at quasirandom positions (that is, eight humps of form (7)), with $s = 1.11$ (not shown). Over a nonuniform bed, the initial solitons evolve to a random wave field consisting of quasisolitonic coherent structures of different heights, together with noncoherent waves. After a sufficiently long time, the smooth nonuniformity resulted in the appearance of tall extreme wave events (Figs. 8–10), when the strongest, oppositely propagating quasisolitonic coherent structures collided. The highest wave events were observed near the left wall, where the depth is minimal.

In the second nonuniform case, we took the function $Z(\zeta)$ as a sum of several Fourier harmonics,

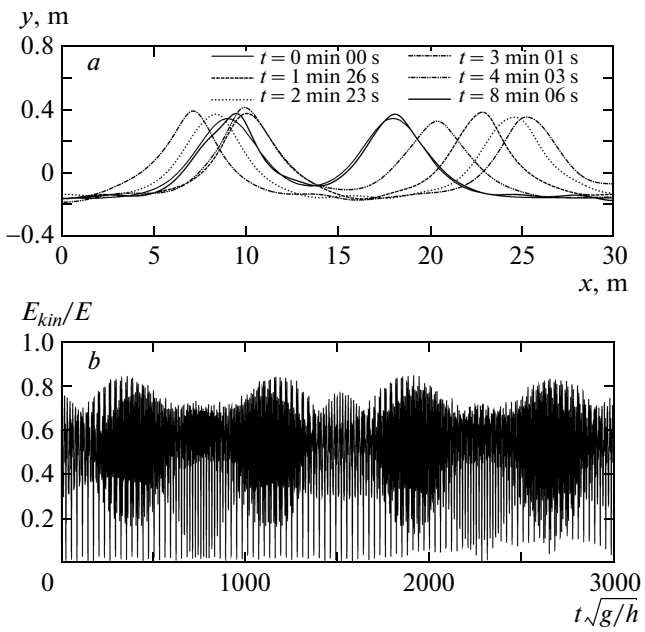

Fig. 5. Two pairs of solitons with equal parameters are present in the system ($L = 60$ m, $h = 1.0$ m): a — wave profiles at several time moments when the solitons collide; b — the ratio of the kinetic energy to the total energy

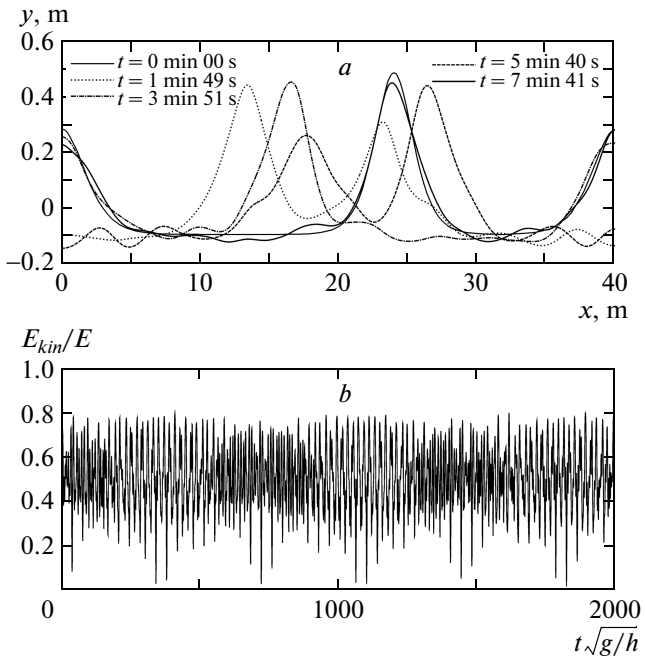

Fig. 6. Two pairs of solitons with different parameters are present in the system ($L = 80$ m, $h = 1.0$ m; a and b show the same quantities as in Fig. 5)

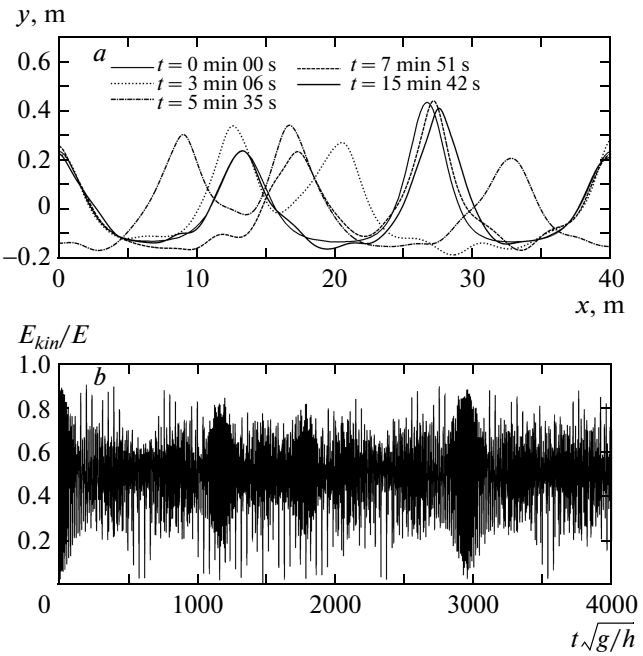

Fig. 7. More complicated regime of the FPU recurrence ($L = 80$ m, $h = 1.0$ m). Three pairs of solitons are present, with one pair stronger than the other two (a and b show the same quantities as in Fig. 5)

$$Z_2(\zeta) = \zeta - \frac{2\pi i}{400} + i\sum_{m=1}^{8}(-1)^m C_m \exp(ik_m\zeta), \qquad (9)$$

with some positive coefficients C_m and positive integer wave numbers k_m. In this case, the bed profile looks practically as a quasirandom, relatively short-correlated curve (Fig. 11). Again, extreme waves appeared at a later stage of the evolution, after the initial state consisting of eight pairs of colliding solitons with parameters $s = 1.12$. Compared to the mild slope, the extreme waves were no so high, but very sharp and typically more asymmetric. We also note that in this case, a typical time of the transition to a random wave field, characterized by a rough profile of the free surface, was much shorter than in the case of a mild-slope bottom. Also, quasisolitonic coherent structures in the second case were relatively short-lived, while a noncoherent part of the wave flied was more developed.

In the third nonuniform case, the bed inhomogeneity was taken in the form of 25 randomly placed nearly identical barriers (the shape of barriers is seen in Fig. 12),

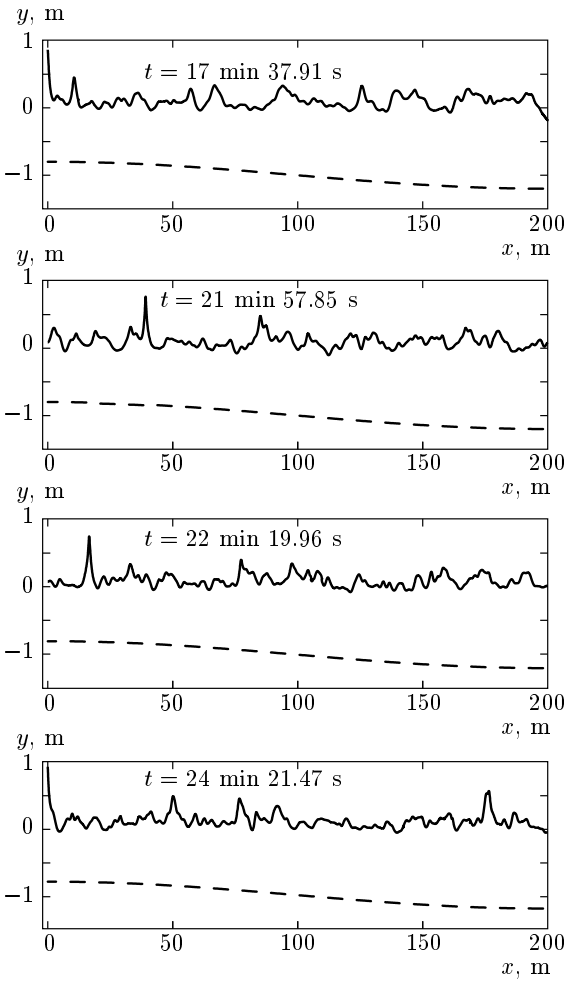

Fig. 8. Rogue waves appear over a mild-slope bed, some of them near the wall: solid and dashed lines are for a free surface and a bottom, respectively

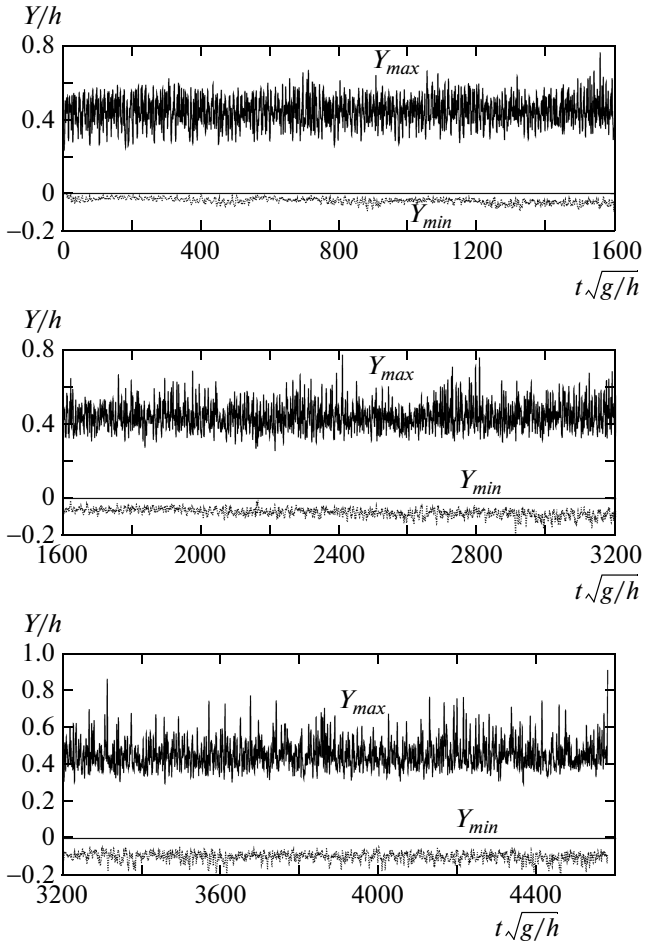

Fig. 9. Maximum and minimum elevations of the free surface over the mild-slope bed

$$Z_3(\zeta) = \zeta - \frac{2\pi i}{400} + \\ + \sum_n \Big\{ i \left[\nu \exp[-B(\zeta + i\varepsilon - \zeta_n)^2] - (\zeta + i\varepsilon - \zeta_n)^2 \right]^{1/2} - \\ - (\zeta + i\varepsilon - \zeta_n) \Big\}, \quad (10)$$

where ζ_n, $n = 0, \ldots, 24$, are quasirandom real numbers in the range from 0 to π, and $\zeta_{n+25} = 2\pi - \zeta_n$ (required for the symmetry). The other parameters were $B = 1400$, $\varepsilon = 0.001$, and $\nu = 5.0 \cdot 10^{-5}$. In contrast to the previous two examples, the conformal mapping corresponding to the function $Z_3(\zeta)$ has singularities in the upper half-plane of the complex variable ζ; however, all the singularities are far enough above the free surface. The large value of the parameter B allowed us to take only several nearest barriers into account when numerically evaluating the function $Z(\zeta)$, thus significantly reducing the computational cost compared to many different possible choices for barrier shapes.

Eight initial pairs of solitons had $s = 1.11$. In this numerical experiment, extreme waves appeared as well (see Fig. 12). Some of them were quite tall, while others had a moderate height, but a very sharp crest (these were essentially asymmetric). In general, the third case is much similar to the second case (compare Fig. 12 and Fig. 11).

4. SUMMARY AND DISCUSSION

In this work, highly accurate numerical simulations of the exact equations of motion for planar potential flows of a perfect fluid with a free surface were used to demonstrate that shallow-water dispersive waves with moderate amplitudes $A/h \lesssim 0.12$ can exhibit the FPU recurrence in a finite basin for various initial states.

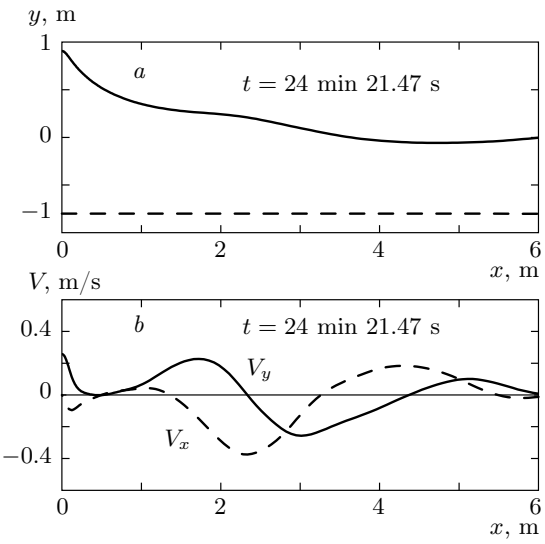

Fig. 10. Big wave over the mild-slope bed near the wall: a — the shape of the free surface (solid curve; the dashed curve is for the bottom); b — velocity distribution along the free surface

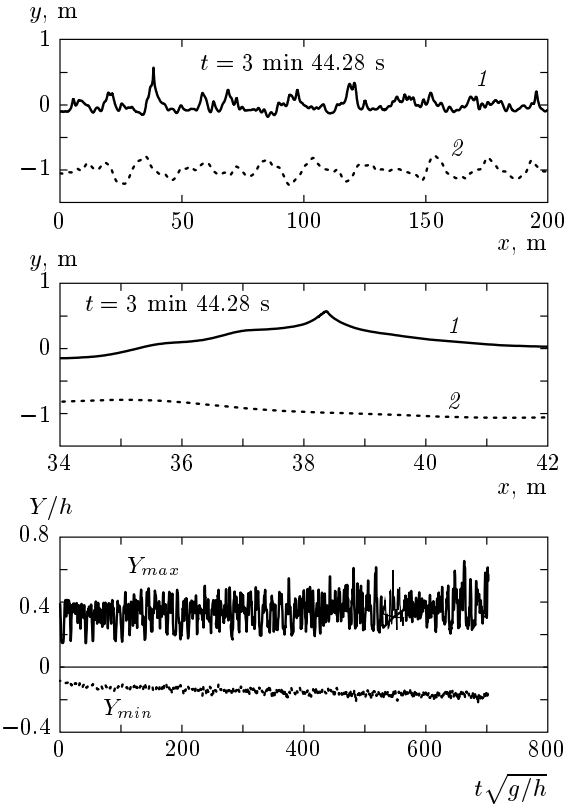

Fig. 11. Formation of a sharp wave over a quasirandom bed (curves *1* and *2* are for a free surface and a bottom, respectively)

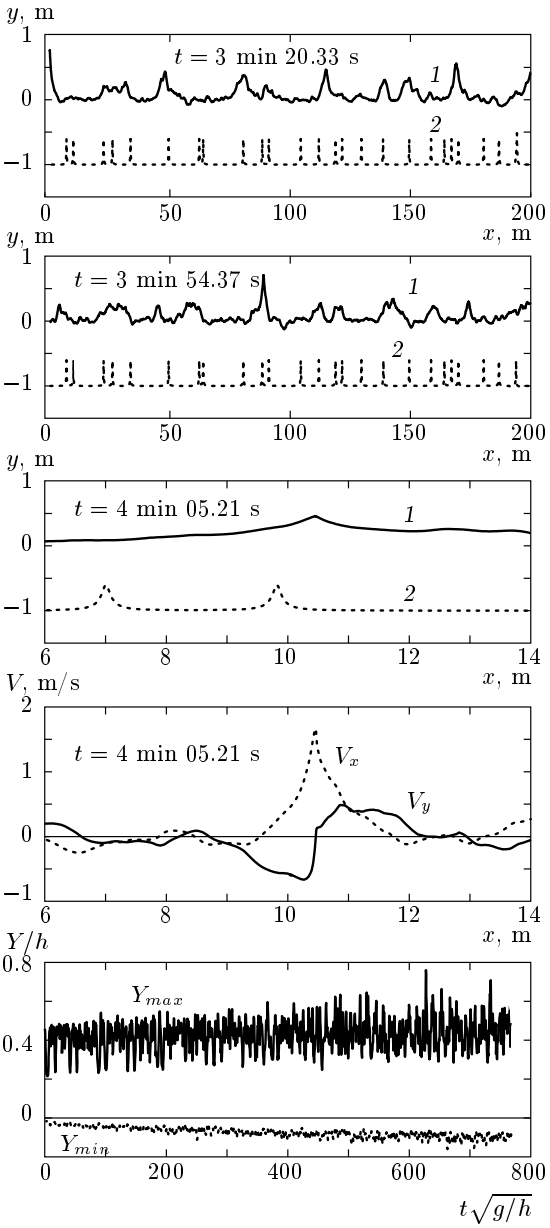

Fig. 12. Formation of extreme waves over a bed with randomly placed barriers (curves *1* and *2* are for a free surface and a bottom, respectively)

However, the best quality of the recurrence is observed for the initial free surface of the form

$$\eta_0(x) = A_0 \cos(2\pi x/L), \quad \psi_0(x) = 0.$$

In that special case, velocities of all the arising solitons appear self-consistently tuned to their phase shifts in mutual collisions, which results in a remarkably perfect recurrence to the initial state even in quite long flumes. A mathematical reason for this self-consistency is not

clear at the moment. The FPU quasirecurrence is also robust with initial states in the form of two solitons. For a larger number of solitons, quasirecurrence is possible with special values of parameters only.

All our numerical results are based on the inviscid theory. In reality, of course, a viscous friction acts against the recurrence. However, it was estimated in [25] that a relative effect of the viscous friction near the bottom and near the side walls of the flume becomes small if all the spatial scales increase proportionally.

In the quasi-integrable regime over a flat horizontal bed, with initial states in the form of several nearly equal solitons, formation of extreme waves appears effectively suppressed, because the solitons preserve their strengths for a long time. When the approximate integrability is destroyed by the bed nonuniformity, the system evolves to a random-wave-field regime where quasisolitonic coherent structures of different amplitudes are present, some of them being stronger than the initial solitons. When the strongest oppositely propagating structures collide, fairly extreme waves arise. The highest extreme waves were observed for a mild-slope bed profile, while for relatively short-correlated bed inhomogeneities, the extreme waves were typically less tall but more sharp-crested. Similar effects were observed both for waves between the vertical walls and for waves with periodic boundary conditions without the additional symmetry.

Our present results for extreme events in bidirectional wave fields over nonuniform beds may have some relevance to the problem of rogue (freak) waves in coastal zone, but only if the coast is in the form of a wave-reflecting cliff rather than a wave-absorbing beach.

This paper was supported by the Russian Foundation for Basic Research (Project № 09-01-00631), the Council of the President of the Russian Federation for Support of Young Scientists and Leading Scientific Schools (Project № NSh-6885.2010.2), and the Presidium of the Russian Academy of Sciences (program "Fundamental Problems of Nonlinear Dynamics").

APPENDIX

A single soliton between the walls in the Boussinesq model

The Boussinesq equations for weakly nonlinear, weakly dispersive long water waves in the dimensionless variables ($\eta/h \to \eta$, $\sqrt{3}x/2h \to x$, $\sqrt{3g/h}\,t/2 \to t$) take the form

$$u_t + uu_x + \eta_x = 0, \tag{A.1}$$

$$\eta_t + [(1+\eta)u]_x + \frac{1}{4}u_{xxx} = 0, \tag{A.2}$$

where η is the vertical displacement of the free surface and $u = \psi_x$ is the horizontal velocity. Following [23], we transform the above system to a more symmetric form

$$q_t + \frac{1}{2}q_{xx} + q^2 r = 0, \tag{A.3}$$

$$-r_t + \frac{1}{2}r_{xx} + r^2 q = 0, \tag{A.4}$$

where new real unknown functions $q(x,t)$ and $r(x,t)$ express the old functions $\eta(x,t)$ and $u(x,t)$ in the following manner:

$$u = \frac{q_x}{q}, \quad \eta = -1 + qr + \frac{u_x}{2}. \tag{A.5}$$

We note that system of equations (A.3) and (A.4) is formally similar to the focusing nonlinear Schrödinger equation

$$2i\psi_t + \psi_{xx} + 2\psi^2\psi^* = 0$$

and its complex conjugate

$$-2i\psi_t^* + \psi_{xx}^* + 2\psi^{*2}\psi = 0.$$

Therefore, we can apply a simple generalization of the Akhmediev–Eleonskii–Korneev–Kulagin ansatz [8, 34, 35], and seek a solution of Eqs. (A.3)–(A.4) in the form

$$(q,r) = [U(x,t) \pm \sqrt{Z(t)}]\exp(\pm P(t)).$$

In this way, we can obtain and integrate a system of equations for the unknown functions $U(x,t)$, $Z(t)$, and $P(t)$. At some point, the problem is reduced to the analysis of two equations (cf. [34])

$$\dot{Z}^2 - 16Z^4 + 16wZ^3 - 4(h+w^2)Z^2 - 4bZ = 0, \tag{A.6}$$

$$U_x^2 + U^4 + 2(w-3Z)U^2 + 2\frac{\dot{Z}}{\sqrt{Z}}U + \\ + (2wZ - 3Z^2 - b) = 0, \tag{A.7}$$

where w, h, and b are some constants (there is also the third equation $\dot{P} + 2Z = w$).

However, we prefer not to deal with a function of two variables such as $U(x,t)$, and therefore use a slightly less general ansatz that still admits physically interesting solutions, with the variables separated from the very beginning:

$$q(x,t) = F(t) + \frac{Q(t)}{D(x) + A(t)}, \tag{A.8}$$

$$r(x,t) = G(t) + \frac{R(t)}{D(x) + A(t)}. \tag{A.9}$$

We take the only x-dependent function $D(x)$ satisfying the relations

$$D_x^2 = 4\mu^2(D^2-1)(1-\epsilon^2 D^2) \equiv cD^2 - \delta D^4 - \beta, \tag{A.10}$$

$$D_{xx} = cD - 2\delta D^3, \tag{A.11}$$

where μ, ϵ, c, and δ are some real parameters. Therefore, it is one of the Jacobi elliptic functions (for their definitions and properties, see, e.g., [36]):

$$D(x) = \mathrm{nd}\left(2\mu x, \sqrt{1-\epsilon^2}\right). \tag{A.12}$$

The x-period of this function is $\tilde{L} = I(\epsilon)/\mu$, where

$$I(\epsilon) = \int\limits_1^{1/\epsilon} \frac{dz}{\sqrt{(z^2-1)(1-\epsilon^2 z^2)}}. \tag{A.13}$$

We now substitute ansatz (A.8)–(A.9) in system (A.3)–(A.4). Using relations (A.10) and (A.11), we obtain the following set of equations (whose left-hand sides are coefficients in front of different powers $(D+A)^{-n}$, $n = 0, 1, 2, 3$, or their linear combinations):

$$\dot{F} + F^2 G + \delta A Q = 0, \tag{A.14}$$

$$-\dot{G} + FG^2 + \delta A R = 0, \tag{A.15}$$

$$\dot{Q} + \frac{Q}{2}(c - 6\delta A^2) + 2QFG + RF^2 = 0, \tag{A.16}$$

$$-\dot{R} + \frac{R}{2}(c - 6\delta A^2) + 2RFG + QG^2 = 0, \tag{A.17}$$

$$2\dot{A} + QG - RF = 0, \tag{A.18}$$

$$-(cA - 2\delta A^3) + QG + RF = 0, \tag{A.19}$$

$$(cA^2 - \delta A^4 - \beta) + QR = 0. \tag{A.20}$$

(The last equation actually appears twice.) It is easy to show that the two algebraic relations are consistent with the five differential equations. It also follows from these equations that

$$FG = \delta A^2 + \gamma, \tag{A.21}$$

where γ is a constant. We now take the squared equation for $\dot{A}$ and obtain

$$4\dot{A}^2 = (RF - QG)^2 = (RF + QG)^2 - 4FGQR = \\ = (cA - 2\delta A^3)^2 + 4(\gamma + \delta A^2)(cA^2 - \delta A^4 - \beta),$$

which is an easily solvable first-order equation

$$4\dot{A}^2 = -4\gamma\delta A^4 + A^2(c^2 + 4c\gamma - 4\beta\delta) - \\ - 4\gamma\beta \equiv 4\gamma\delta(A^2 - \alpha_1^2)(\alpha_2^2 - A^2), \tag{A.22}$$

where

$$\alpha_{1,2}^2 = \frac{1}{2}\left(\frac{c^2}{4\gamma\delta} + \frac{c}{\delta} - \frac{\beta}{\gamma}\right) \mp \\ \mp \sqrt{\frac{1}{4}\left(\frac{c^2}{4\gamma\delta} + \frac{c}{\delta} - \frac{\beta}{\gamma}\right)^2 - \frac{\beta}{\delta}}. \tag{A.23}$$

The solution of Eq. (A.22) is again expressed through an elliptic function:

$$A(t) = \alpha_1 \,\mathrm{nd}\left(t\alpha_2\sqrt{\gamma\delta}, \sqrt{1 - \left(\frac{\alpha_1}{\alpha_2}\right)^2}\right) \equiv \\ \equiv \alpha_1 \,\mathrm{nd}\,(\xi, \kappa)\,. \tag{A.24}$$

Because $\mathrm{nd}(\xi,\kappa) = 1/\mathrm{dn}(\xi,\kappa)$ by definition (see [36]) and $[\mathrm{dn}(\xi,\kappa)]_\xi = -\kappa^2 \mathrm{sn}(\xi,\kappa)\,\mathrm{cn}(\xi,\kappa)$, we can express the time derivative $\dot{A}(t)$ as

$$\dot{A}(t) = \alpha_1\alpha_2\sqrt{\gamma\delta}\kappa^2 \mathrm{sd}(\xi,\kappa)\,\mathrm{cd}(\xi,\kappa). \tag{A.25}$$

Thus, we have obtained explicit expressions for the quantities A, QR, FG, and $(RF + QG)$. From these, we can also extract the ratios Q/F and R/G, because

$$\frac{R}{G} + \frac{Q}{F} = \frac{RF + QG}{FG} = \frac{cA - 2\delta A^3}{\delta A^2 + \gamma}, \tag{A.26}$$

$$\frac{R}{G} - \frac{Q}{F} = \frac{2\dot{A}}{FG} = \frac{2\dot{A}}{\delta A^2 + \gamma}. \tag{A.27}$$

The obtained information is sufficient to construct the velocity $u(x,t)$ and the free surface elevation $\eta(x,t)$ via formulas (A.5), because

$$u = \left(\frac{1}{D+A+Q/F} - \frac{1}{D+A}\right) D_x, \qquad (A.28)$$

$$\eta = -1+FG+\frac{RF+QG}{D+A}+\frac{QR}{(D+A)^2}+\frac{u_x}{2}. \qquad (A.29)$$

Using the relations $c = 4\mu^2(1+\epsilon^2)$, $\delta = 4\mu^2\epsilon^2$, and $\beta = 4\mu^2$, it can be shown that $\alpha_1 < 1$ and $\alpha_2 > 1/\epsilon$, and therefore at definite time moments the function $A(t)$ takes values $A_1 = 1$ or $A_2 = 1/\epsilon$. Simultaneously, at those time moments, either $Q = 0$ or $R = 0$. When $Q = 0$, the velocity field $u(x)$ is zero everywhere, while the free surface profile is either $\eta_1(x)$ or $\eta_2(x)$, where

$$\eta_1(x) = -1 + \gamma + 4\mu^2\left(\epsilon^2 + \frac{1-\epsilon^2}{D(x)+1}\right), \qquad (A.30)$$

$$\eta_2(x) = \eta_1(x - \tilde{L}/2). \qquad (A.31)$$

We see that the best choice for the constant γ is $\gamma = 1-4\mu^2\epsilon$, because in this case $\eta_{1min} = 0$. The function $\eta_1(x)$ has a single hump at $x = 0$, and therefore corresponds to the moments when a soliton collides with the left wall, while $\eta_2(x)$ corresponds to the collisions of the soliton with the right wall at $x = \tilde{L}/2$.

In the limit $\epsilon \ll 1$, we have $\tilde{L} \to \infty$ and $D(x) \approx \mathrm{ch}(2\mu x)$, and hence

$$\eta_1(x) \approx \frac{4\mu^2}{1+\mathrm{ch}(2\mu x)} = \frac{2\mu^2}{\mathrm{ch}^2(\mu x)}. \qquad (A.32)$$

The full solution in this limit is given by the following formulas (it is interesting to note that the solution below is essentially Eq. (52) in Ref. [34] for the focusing nonlinear Schrödinger equation, but evaluated at imaginary time):

$$q(x,t) = \left[1 + \frac{2\mu^2\,\mathrm{ch}\left(2t\mu\sqrt{1+\mu^2}\right) - 2\mu\sqrt{1+\mu^2}\,\mathrm{sh}\left(2t\mu\sqrt{1+\mu^2}\right)}{\sqrt{1+\mu^2}\,\mathrm{ch}(2\mu x) + \mathrm{ch}\left(2t\mu\sqrt{1+\mu^2}\right)}\right] e^{-t}, \qquad (A.33)$$

$$r(x,t) = \left[1 + \frac{2\mu^2\,\mathrm{ch}\left(2t\mu\sqrt{1+\mu^2}\right) + 2\mu\sqrt{1+\mu^2}\,\mathrm{sh}\left(2t\mu\sqrt{1+\mu^2}\right)}{\sqrt{1+\mu^2}\,\mathrm{ch}(2\mu x) + \mathrm{ch}\left(2t\mu\sqrt{1+\mu^2}\right)}\right] e^{t}. \qquad (A.34)$$

Collision of the soliton with the wall at $x = 0$ occurs at $t = t_*$, when

$$\mathrm{ch}\left(2t_*\mu\sqrt{1+\mu^2}\right) = \sqrt{1+\mu^2}.$$

It is easy to derive that before and after the collision, the soliton (at $x > 0$) moves with the respective velocities $s = \mp\sqrt{1+\mu^2}$.

REFERENCES

1. E. Fermi, J. Pasta, and S. Ulam, Los Alamos Scientific Laboratory Report No. LA-1940, Los Alamos, New Mexico (1955).
2. N. J. Zabusky and M. D. Kruskal, Phys. Rev. Lett. **15**, 240 (1965).
3. V. E. Zakharov, Zh. Eksp. Teor. Fiz. **65**, 219 (1973).
4. A. Thyagaraja, Phys. Fluids **22**, 2093 (1979).
5. H. C. Yuen and W. E. Ferguson, Phys. Fluids **21**, 1275 (1978).
6. E. Infeld, Phys. Rev. Lett. **47**, 717 (1981).
7. H. C. Yuen and B. M. Lake, Adv. Appl. Mech. **22**, 67 (1982).
8. N. N. Akhmediev and V. I. Korneev, Theor. Math. Phys. **69**, 1089 (1986).
9. Q. Zhu, Y. M. Liu, and D. K. P. Yue, J. Fluid Mech. **496**, 213 (2003).
10. A. R. Osborne, M. Onorato, M. Serio, and L. Bergamasco, Phys. Rev. Lett. **81**, 3559 (1998).
11. R. Camassa and L. Lee, J. Comp. Phys. **227**, 7206 (2008).
12. G. Van Simaeys, Ph. Emplit, and M. Haelterman, Phys. Rev. Lett. **87**, 033902 (2001).
13. N. J. Zabusky, Chaos **15**, 015102 (2005).
14. G. P. Berman and F. M. Izrailev, Chaos **15**, 015104 (2005).

15. V. E. Zakharov, J. Appl. Mech. Tech. Phys. **9**, 190 (1968).

16. M. P. Tulin and T. Waseda, J. Fluid Mech. **378**, 197 (1999).

17. J. B. Song and M. L. Banner, J. Phys. Oceanogr. **32**, 2541 (2002).

18. W. S. Chiang and H. H. Hwung, Phys. Fluids **19**, 014105 (2007).

19. S. Leblanc, Eur. J. Mech. B/Fluids **28**, 605 (2009).

20. D. J. Kaup, Progr. Theor. Phys. **54**, 396 (1975).

21. B. A. Kupershmidt, Comm. Math. Phys. **99**, 51 (1985).

22. A. O. Smirnov, Theor. Math. Phys. **66**, 19 (1986).

23. J. E. Zhang and Y. Li, Phys. Rev. E **67**, 016306 (2003).

24. W. Craig, P. Guyenne, J. Hammack et al., Phys. Fluids **18**, 057106 (2006).

25. V. P. Ruban, Pis'ma v Zh. Eksp. Teor. Fiz. **93**, 213 (2011).

26. V. P. Ruban, Phys. Rev. E **70**, 066302 (2004).

27. V. P. Ruban, Phys. Rev. E **77**, 037302 (2008).

28. E. Pelinovsky and C. Kharif (editors), Eur. J. Mech. B/Fluids **25**, 535–692 (2006).

29. N. Akhmediev and E. Pelinovsky (editors), The Eur. Phys. J.–Special Topics **185**, 1–266 (2010).

30. E. Pelinovsky and C. Kharif (editors), Special Issue "Extreme and Rogue Waves", Natural Hazards and Earth System Sciences (2010); http://www.nat-hazards-earth-syst-sci.net.

31. V. P. Ruban, Phys. Lett. A **340**, 194 (2005).

32. V. P. Ruban, Phys. Rev. E **77**, 055307(R) (2008).

33. V. P. Ruban, Phys. Rev. E **78**, 066308 (2008).

34. N. N. Akhmediev, V. M. Eleonskii, and N. E. Kulagin, Theor. Math. Phys. **72**, 809 (1987).

35. N. Akhmediev and A. Ankiewicz, Phys. Rev. A **47**, 3213 (1993).

36. E. T. Whittaker and G. N. Watson, *A Course of Modern Analysis*, Part 2, Cambridge University Press (1927).